Reaction Kinetics, Mechanisms and Catalysis (2021) 132:155–170
https://doi.org/10.1007/s11144-020-01919-0

Inverse ZnO/Cu catalysts for methanol synthesis from CO_2 hydrogenation

Guihui Wang[1] · Fei Luo[1] · Lili Lin[1] · Fuzhen Zhao[1]

Received: 2 October 2020 / Accepted: 27 December 2020 / Published online: 8 January 2021

Abstract

A series of inverse ZnO/Cu catalysts were prepared with varied Zn/Cu ratios using a microemulsion method. The catalysts were tested for CO_2 hydrogenation to methanol and the structure was characterized by nitrogen physisorption, X-ray diffraction (XRD), X-ray photoelectron spectroscopy (XPS), Transmission electron microscopy (TEM), Scanning electron microscope (SEM), H_2 temperature-programmed reduction (H_2-TPR) and H_2 temperature-programmed desorption (H_2-TPD). On the inverse samples, less amount of highly dispersed Cu was observed than that of the conventional Cu/ZnO catalysts. Thus, the inverse ZnO/Cu catalysts showed a lower CO selectivity and a higher methanol selectivity. CuZn alloy was formed in the samples, in which ZnO/Cu(4:6) had the most amount of the CuZn alloy. A linear relationship between the methanol yield and the CuZn alloy content can be found for the ZnO/Cu catalysts. Among all the catalysts, ZnO/Cu(4:6) exhibited the highest CH_3OH yield (2.8 mmol g^{-1} h^{-1}) at 2.0 MPa and 250 °C, much higher than the conventional Cu/ZnO catalyst with the same composition. Moreover, microemulsion method is a very effective method to tune particle size of the catalysts.

Keywords CO_2 hydrogenation · Methanol · ZnO/Cu catalysts · CuZn alloy

Introduction

Under the background of global warming, the "low-carbon economy" based on low energy consumption and low output of greenhouse gas has become a hotspot. Converting the emitted CO_2, the major greenhouse gas, into valuable chemicals is

Supplementary information The online version of this article (https://doi.org/10.1007/s11144-020-01919-0) contains supplementary material, which is available to authorized users.

✉ Fuzhen Zhao
32113505@qq.com; fzzhao@mail.scuec.edu.cn

[1] Key Laboratory of Catalysis and Energy Materials Chemistry of Ministry of Education & Hubei Key Laboratory of Catalysis and Materials Science, South-Central University for Nationalities, Wuhan 430074, China

a subject that many researchers have been working on. Methanol, as an important industrial commodity [1] as well as an ideal clean synthetic fuel [2], becomes the preferred target product for CO_2 conversion. CO_2 hydrogenation to methanol is expected to solve both environmental and energy issues at the same time. Therefore, much attention has been attracted on this research field.

At present, $Cu/ZnO/Al_2O_3$ catalyst has been extensively studied for CO_2 hydrogenation and industrialized for several decades in methanol production from syngas [3]. Although $Cu/ZnO/Al_2O_3$ shows excellent performance using syngas as feed gas, it is less active in CO_2 hydrogenation to methanol [4]. In order to improve the activity, researchers have conducted in-depth researches such as adjusting the size of Cu clusters [5, 6], optimizing the preparation methods [7–9] and adding promoters [10, 11]. Recently, a layer of metastable ZnO was clearly observed on the top of Cu particles for some Cu/ZnO catalysts with high performance for CO_2 hydrogenation [12, 13]. This ZnO layer can not only form ZnO_x species acting as cocatalysts but also can protect the Cu from reshaping and sintering during the reaction [12]. This kind of catalysts with the oxide-metal structure was first proposed as "inverse catalysts" by Rodriguez et al.[14].

Due to the unique structure of the inverse catalysts, they showed better performance than conventional catalysts in some reactions, such as CO oxidation [15], partial oxidation of methanol [16] and water–gas shift reaction [14]. For CO_2 hydrogenation to methanol, some inverse catalysts, e.g. ZnO/Cu(100) [17] and $MnOx/Co_3O_4$ [18], exhibited superior activity than that of Cu/ZnO $(000\bar{1})$ and $CoOx/MnO_2$. In order to further investigate the influence of composition on the properties and catalytic performance of the powder ZnO/Cu catalysts, we used microemulsion method to prepare a series of ZnO/Cu catalysts and investigated their performance for CO_2 hydrogenation to methanol. Our results indicated that the inverse ZnO/Cu showed higher methanol selectivity than the conventional Cu/ZnO sample.

Experimental

Catalysts preparation

The catalysts were prepared with a microemulsion method. First, two microemulsions with the same composition were prepared. Both of them contained 32% wt. of Trition-x-100 as the surfactant, 20% of n-hexanol as the cosurfactant, 38% of n-heptane as the oil phase and 10% water. In one of the microemulsion, an appropriate amount of copper nitrate was dissolved in the water phase, while an appropriate amount of precipitating agent (tetramethylammonium hydroxide, TMAH) was added to the other microemulsion. After stirring for 1 h, the TMAH-containing microemulsion was added dropwise to the microemulsion containing copper nitrate. The mixture was kept at 25 °C for 24 h to complete the precipitate. Then, the precipitate was separated with a centrifuge for 3 times and washed with methanol. After dried in an oven at 100 °C for 24 h and calcined at 350 °C in a muffle for 2 h, CuO was finally obtained.

ZnO/CuO precursors were prepared in the same procedure except that the above-obtained CuO and zinc nitrate were added to the water phase in one of the micro-emulsions. After precipitation, centrifugal separation, drying, calcination at 350 °C for 2 h, and finally reduced under pure hydrogen at 300 °C for 2 h, ZnO/Cu catalysts were obtained. A series of ZnO/Cu catalysts were obtained where n(Zn)/n(Cu) equals to 1:9, 2:8, 3:7, 4:6 and 5:5.

For comparison, CuO/ZnO sample, with a n(Zn)/n(Cu) of 4:6, was also prepared using the same method. After reducing under pure hydrogen at 300 °C for 2 h, Cu/ZnO (6:4) was obtained.

Catalysts characterization

N_2 adsorption–desorption was measured at liquid nitrogen temperature (77 K) on a Quantachrome Autosorb-1-C-TCD-MS instrument. Prior to the tests, evacuating of the samples for 6 h at 200 °C was carried out. Multipoint Brunauer–Emmett–Teller (BET) model and Barrett-Joyner-Halenda (BJH) model were applied to calculate the specific surface areas (S_{BET}) and the pore size distributions.

The phase analysis of the catalyst was carried out on a Brucker Advance D8 X-ray powder diffractometer (XRD). Cu-Kα with a wavelength of 0.1506 nm was used as the radiation source. The instrument was operating at 40 kV and 40 mA, with a scanning range of 20°–80° (0.0167°/step).

X-ray photoelectron spectroscopies were collected on a VG Mulitilab 2000 instrument (Thermal Electron Corporation) under 2×10^{-6} Pa. Monochromatic Al K_α X-ray operating at 15 kV and 20 mA was used as the radiation source. Samples were first reduced in pure H_2 at 300 °C for 2 h. After cooled down to room temperature in pure H_2, they were sealed in the glass sample bottles without air. Finally, the samples were transferred into the XPS instrument for and measurement. The C1s binding energy (284.6 eV) was used as a standard to calibrate the shift of the binding energy caused by the charge effect.

TEM images were obtained on FEI Tecnai G^2 F20 electron microscope under 200 kV. Scanning electron microscope (SEM) images of the sample were acquired on a Hitachi-48005 instrument equipped with energy dispersive X-ray analysis (EDX) detector.

The reducibility of the catalysts was tested on a multifunctional characterization analyzer AMI-200 (Zeton Altamira Corporation). 25 mg of the catalyst was purged at 150 °C for 1 h under argon (25 mL/min) to remove the adsorbed water. After cooling down to 50 °C, 10% H_2/90% Ar with a flow rate of 25 mL/min was used to reduce the sample. H_2-TPR data was collected with the temperature rising to 400 °C at a heating ramp of 10 °C/min.

H_2-TPD was performed on the Micromeritics Instruments Corporation Auto-Chem II 2920 instrument to determine the Cu surface area and the dispersion of Cu. 0.2 g of a sample was first reduced in a pure hydrogen (35 mL/min) atmosphere. The temperature was raised from room temperature to 300 °C at a heating rate of 10 °C/min and held at 300 °C for 2 h. After cooling down to -50 °C and holding at this temperature for 1 h in pure hydrogen, pure Ar (25 mL/min) was introduced into the

system. Then, the temperature was raised from -50 °C to 150 °C in the Ar at a heating rate of 10 °C/min. Assuming that the chemisorption of H_2 on Cu atoms is carried out according to Cu:H = 2:1 [19, 20], the specific copper surface area (S_{Cu}) and the degree of dispersion (D) were calculated as follows:

$$S_{Cu} = 4 \times H_2\text{uptake} \times N_{av}/(1.47 \times 10^{19})(m^2 - Cu/g)$$

In this equation, N_{av} is the Avogadro's constant, 1.47×10^{19} is the value of Cu atoms per square meter [19, 21].

$$\text{Percentage dispersion (D)} = \frac{\text{amount of Cu atoms on surface (moles)}}{\text{total amount of Cu atoms in the sample(moles)}} \times 100\% = \frac{H_2 \text{ uptake} \times 4\text{(moles)}}{\text{total amount of Cu atoms in the sample(moles)}} \times 100\%$$

Catalytic performance measurements

CO_2 hydrogenation to methanol activity measurements were carried out in a stainless-steel high-pressure reaction device. 0.1 g of a sample was loaded in the fix-bed reactor with a diameter of 6 mm. Before the activity tests, the sample was first reduced in pure H_2 with a GHSV of 2.4 L h^{-1} g^{-1} at 300 °C for 2 h under atmospheric pressure and then cooled to room temperature. The typical gas ($n(CO_2)$/$n(H_2)$ = 1:3) with a GHSV of 3.6 L h^{-1} g^{-1} was injected into the device. The catalytic performance test was conducted at 2 MPa and 250 °C and lasted for 50 h for each sample.

The final gas components were analyzed online by Agilent Micro GC 3000A gas chromatograph (TCD detector). The methanol and water components in the product were collected by a 0 °C cold trap, and analyzed offline with an Agilent GC 4890D (FID detector).

Results and discussion

Textural properties

Fig. 1 displays the nitrogen adsorption–desorption isotherms and pore sizes distributions of the ZnO/Cu catalysts. All samples, showed a type IV isotherm, which was the typical feature of mesoporous materials. It could also be seen that all samples had a H3 type hysteresis loop, resulted from the capillary condensation inside slit-like pores formed by aggregation of flaky particles [22]. From Fig. 1b, one can observe that ZnO/Cu (5:5) and ZnO/Cu (4:6) samples had two distinct peaks, indicating a bimodal pore size distribution. The pore structure parameters, including the BET specific area (S_{BET}), total pore volume (V_p) and pore size (D_{BJH}) are listed in Table 1. ZnO/Cu (3:7) had the largest specific surface area, which was beneficial to

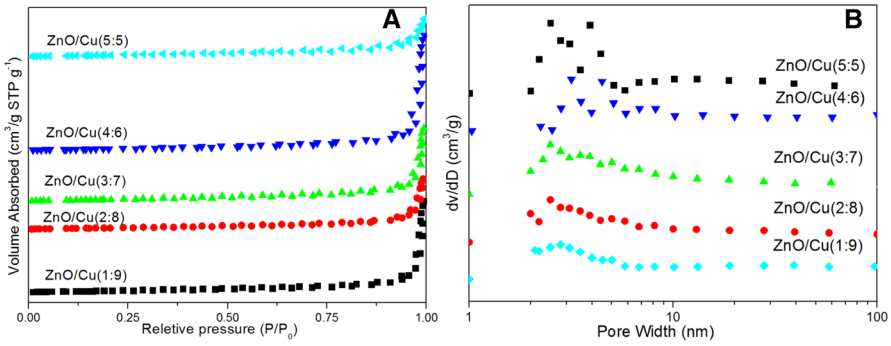

Fig. 1 N_2 adsorption–desorption isotherms (**a**) and the BJH pore size distribution (**b**) at 77 K for the reduced ZnO/Cu catalysts

the dispersion of active components. However, due to the small pore size, the pore volume was relatively small. ZnO/Cu(4:6) had the largest pore volume and pore size.

XRD measurements

The XRD diffraction patterns for ZnO/Cu catalysts were depicted in Fig. 2. As mentioned in the preparation section, the samples were reduced at 300 °C and ZnO could only be reduced at higher than 400 °C [23]. Therefore, only ZnO and Cu species could be detected for all ZnO/Cu catalysts. With the increase of Cu content, the intensity of the Cu diffraction peaks was gradually enhanced, while the characteristic diffraction peaks of ZnO were gradually weakened. The particle sizes of ZnO and Cu were calculated using the Scherrer equation at $2\theta = 36.2$ °C and 43.3°. The data are shown in Table 1. Before the reduction process, the particle size of CuO was about 14 nm, obtaining from the XRD pattern (Fig. S1). After the reduction, relatively large Cu particles were formed because of the coalescence of copper component [24]. Cu particle sizes followed this trend: ZnO/Cu(4:6) < ZnO/Cu(5:5) < ZnO/Cu(3:7) < ZnO/Cu(2:8) < ZnO/Cu(1:9). ZnO/Cu(4:6) catalyst had the minimum Cu particle size in the series, probably suggesting the strongest interaction between Cu and ZnO, as observed similarly for the CuO-CeO_2 systems [25]. No obvious difference for ZnO

Table 1 Physicochemical properties and particle sizes of ZnO and Cu for ZnO/Cu catalysts

Sample	S_{BET}(m^2/g)	Vp (cm^3/g)	D_{BJH}(nm)	Cu(nm) [a]	ZnO(nm) [a]	a_{Cu}(Å)
ZnO/Cu(1:9)	51.9	0.48	2.8	29.3	17.0	3.618
ZnO/Cu(2:8)	40.3	0.27	2.5	27.8	19.6	3.622
ZnO/Cu(3:7)	65.5	0.38	2.5	24.2	17.1	3.627
ZnO/Cu(4:6)	56.2	0.60	3.2	19.8	20.7	3.634
ZnO/Cu(5:5)	47.1	0.20	2.5	23.5	20.5	3.628

[a]Calculated from the Scherrer formula

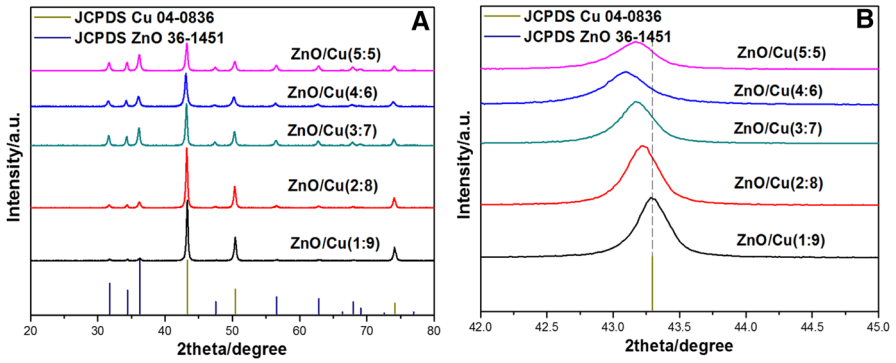

Fig. 2 XRD diffraction patterns of ZnO/Cu catalysts

particles for all the ZnO/Cu samples was observed, as the particle sizes calculated using the Scherrer equation usually have an error of 1 nm [26]. The results indicated that microemulsion method is an effective method to tune particle size of Cu in the catalysts. Moreover, for ZnO/Cu(4:6) sample, the particle sizes of ZnO (20.7 nm) and Cu (19.8 nm) are quite similar. It has been reported that the interface of Cu–ZnO samples has some connection with the particle size of the two components. Although it was impossible to get precise quantification of the interface due to the non-ideal spherical shape, the authors considered that the more similar the particle sizes were, the larger was the interface at the perimeter [27]. Out of these this factor, ZnO/Cu (4:6) sample seemed to have the largest interface. For the other catalysts, the interface showed a decrease trend with the increase of Cu particle sizes. As reported previously, CO_2 mainly adsorbs on the surface of ZnO [11], while H_2 dissociatively adsorbs on the surface of Cu and transfers H atoms to ZnO via spillover. Large interface, i.e. large contact area between ZnO and Cu, can facilitate the spillover of H atoms and thus the formation of methanol.

In order to make sure whether CuZn alloy was formed in the samples, the enlarged part of the XRD patterns from 42–45 ^{o} is shown in Fig. 2b. Clearly, compared with pure Cu pattern, a slight shift of 2θ towards a lower angle can be noticed. Cu lattice constant was calculated using $a_{Cu} = \frac{\sqrt{3}}{2\sin}\theta\lambda$ (cubic structure, orientation (111)). The obtained a_{Cu} is shown in Table 1. The lattice constant of pure Cu (JCPDS Cu 04–0836) was also calculated using the same method and the value is 3.616 Å. The Cu lattice parameters of all the prepared samples were larger than that of pure Cu, indicating an expansion of the Cu lattice [28]. This should be attributed to the fact that Zn^{2+} entered into the Cu lattice to form Cu–Zn alloy, as reported by Valant [29] and Nakamura [30], since Zn^{2+} (0.60 Å) is bigger than Cu^{2+} (0.57 Å) [29]. Generally, the more Zn^{2+} entered into the Cu lattice, the larger the cell parameters of the resulted catalysts would be. Therefore, in the series, ZnO/Cu(4:6) had the most amount of CuZn alloy, followed by ZnO/Cu(5:5), ZnO/Cu(3:7), ZnO/Cu(2:8) and ZnO/Cu(1:9).

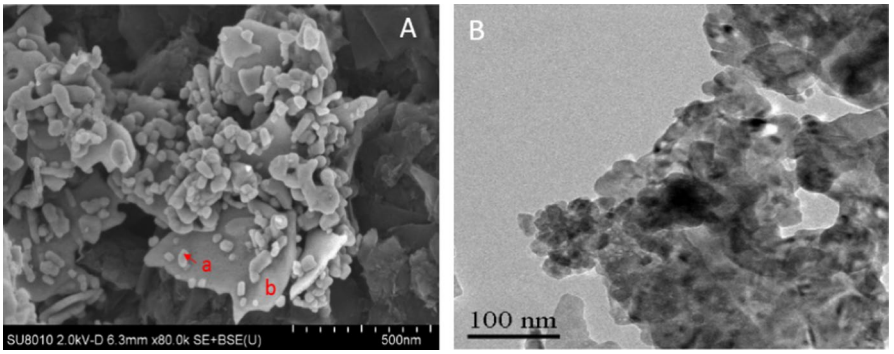

Fig. 3 SEM (**a**) and TEM (**b**) images of ZnO/Cu (4:6) sample

Table 2 EDS analysis for ZnO/Cu (4:6) sample

Element	Cu/wt%	Zn/wt%	O/wt%
Point a	11.88	60.96	27.16
Point b	53.96	17.01	29.04

SEM and TEM

SEM (A) and TEM (B) images of ZnO/Cu (4:6) sample are shown in Fig. 3 and the EDS results are displayed in Table 2. From Table 2, one can see that at point a, Zn element accounts for the majority; while at point b, Cu element accounts for the majority. Combing with the SEM image of the sample, it suggested that the small particles is probably correspond to the ZnO species. Meanwhile, the flake-like structure was probably assigned to Cu particles. Hence, this finding implied that ZnO particles were relatively well-dispersed on the surface of flake-like Cu. The TEM image of the catalyst is consistent with the SEM results. The particle size of Zn in both SEM and TEM images is about 20 nm, in accordance with the XRD results. However, the particle size of Cu seems a little difficult to distinguish due to the aggregation.

XPS measurements

The XPS measurements were performed to determine the valence state of Zn and Cu on the surface and the results are shown in Fig. 4. The binding energy for Zn $2p_{3/2}$ was at about 1021.5 eV, which agrees well with reported Zn^{2+} [13]. There are two main peaks for Cu 2p XPS spectrum. The peaks at binding energy (BE) = 932–933 eV and BE = 952–953 eV should be ascribed to $Cu2p_{3/2}$ and $Cu2p_{1/2}$. For CuO sample, the obvious shake-up satellite peak at 937–945 eV was the characteristic of Cu^{2+} [31]. After the reduction process, the significant

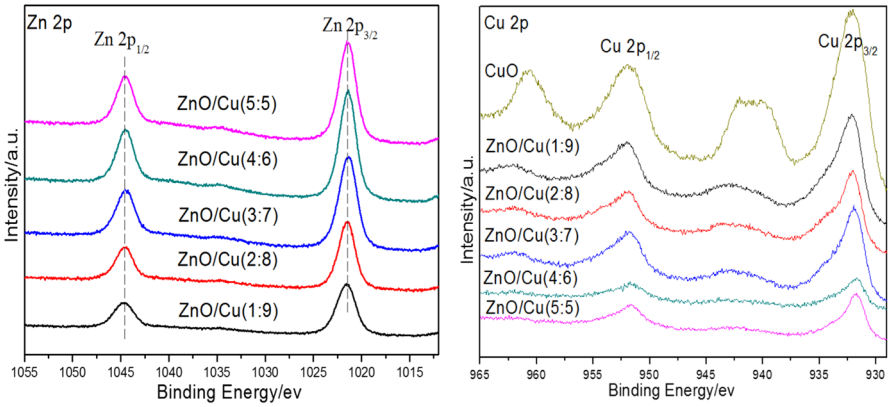

Fig. 4 Zn 2p and Cu2p XPS spectra of CuO and the reduced ZnO/Cu catalysts

decrease or the absence of the shake-up peak strongly suggested that most cupric species had been reduced to a low oxidation or metallic state. Since the binding energy of Cu^+ and Cu^0 are almost the same, XPS spectra could hardly give a distinguished identification. However, our previous study showed that Cu^+ only existed for a short time during the reduction process [32]. There were some other reports on similar catalysts confirmed the presence of only Cu^0 on the surface using Cu LMM spectra [27, 33]. Therefore, we could conclude that Cu^0 was the dominant species on the surface after the reduction. Table 3 lists the Cu/Zn molar ratios both on the surface and in the bulk of the samples given by XPS and Inductively Coupled Plasma (ICP) results. It was obvious that the Cu/Zn ratios on the surface of the catalysts were significantly lower than that in the bulk phase, suggesting that only a little amount of Cu presented on the surface in the prepared catalysts, while large amount of Cu remained in the bulk.

Table 3 Cu/Zn molar ratios, TPR and TPD results for ZnO/Cu catalysts

Sample	XPS[a]	ICP[b]	Lower peak/°C [c]	higher peak/°C [c]	D(%)	S_{Cu} (m^2/g)
ZnO/Cu(1:9)	0.8	9.0	246	268	0.39	1.6
ZnO/Cu(2:8)	0.5	4.0	214	238	0.49	1.7
ZnO/Cu(3:7)	0.4	2.3	220	246	1.04	2.6
ZnO/Cu(4:6)	0.1	1.5	176	212	1.46	3.7
ZnO/Cu(5:5)	0.2	1.0	206	239	0.86	4.0

[a]Cu/Zn molar ratios obtained by XPS

[b]Cu/Zn molar ratios obtained by ICP

[c]The temperatures of different reduction peaks of CuO

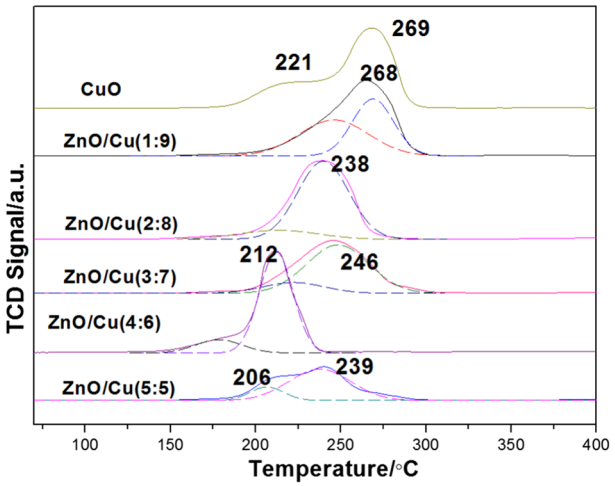

Fig. 5 H_2-TPR profiles for ZnO/Cu catalysts

The reducibility of the catalysts

The TPR profiles of the ZnO/Cu catalysts with different Zn/Cu ratios were presented in Fig. 5. For pure CuO sample, two reduction peaks at about 221 °C and 269 °C were observed, indicating the presence of two different types of CuO. Many researchers have extensively studied the reducibility of CuO. The lower temperature reduction peak was commonly ascribed to the reduction of highly dispersed CuO, while the higher reduction peak was ascribed to the reduction of bulk CuO interacting with the support [34, 35]. Furthermore, the two reduction peaks have also been described as stepwise reduction of copper, which is Cu^{2+} to Cu^{+} and Cu^{+} to metallic Cu [36]. In order to further analyze the reducibility of ZnO/Cu catalysts, the profiles were deconvoluted using the Gaussian Fitting. The reduction temperatures of CuO are shown in Table 3. All ZnO/Cu samples could be divided into two peaks, also suggesting the existence of two different kinds of CuO species or the two reduction steps. After adding ZnO, the position of the CuO reduction peaks shifted to the low temperatures, suggesting that the interaction between ZnO and Cu promoted the reduction of CuO. The most notable peak shift could be seen for ZnO/Cu(4:6) sample, indicating the strongest interaction, which is in accordance with the results of XRD. Meanwhile, the position of the reduction peaks of ZnO/Cu(1:9) did not change much, probably because the content of ZnO was too low to have any effects.

H_2-TPD

The copper surface area (S_{Cu}) was determined using the H_2-TPD method. Although N_2O measurement has been used for about 30 years to calculate the Cu surface area of the Cu/ZnO catalysts, recently, it has been confirmed that this method was not accurate because N_2O measured the Cu surface area as well as the oxygen vacancies

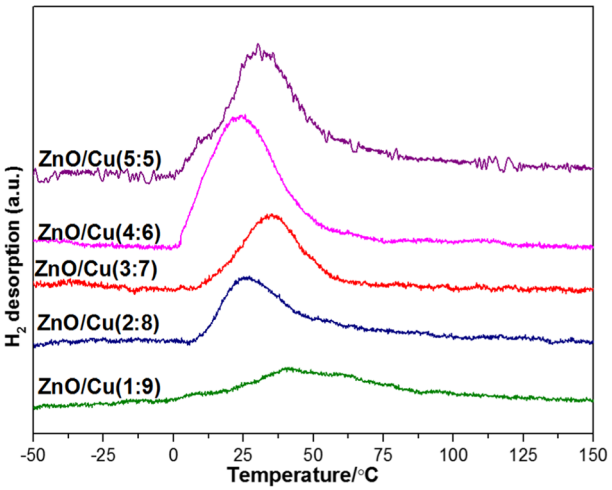

Fig. 6 H_2-TPD profiles for ZnO/Cu samples

on the ZnO surface [20, 37, 38], whereas the real Cu surface area should be accurately determined by H_2-TPD [20, 37, 39]. Fig. 6 gives the profiles for ZnO/Cu samples. As reported previously, pure ZnO did not absorb any hydrogen in our entire test range [20]. Usually, the desorption temperature of H_2 from the ZnO surface was in the range of 300–500 °C [40, 41]. However, Cu species exhibited one desorption peak in the range of 30–60 °C, which can be assigned to the desorbing results of H atoms from metallic Cu surface [42–44]. For all the ZnO/Cu profiles, only one desorption peak at about 30 °C can be detected, which is quite similar to the desorption H_2 from metallic Cu surface. Based on the hydrogen desorption amount, we calculated Cu dispersion (D) and S_{Cu}, which are shown in Table 3. All the ZnO/Cu samples had rather small Cu surface areas and Cu dispersion due to the unique inverse structure. It was observed that for ZnO/Cu catalysts, with the increase of ZnO content from 10 to 50%, the exposed Cu surface area increased from 1.6 m^2/g to 4.0 m^2/g. However, the dispersion of Cu species had a different trend. It increased from 0.39 to 1.46 when ZnO content increased from 10 to 40%. When further increased ZnO content to 50%, a decrease of the dispersion of Cu species to 0.86 can be observed.

Catalytic and stability performance

Fig. 7 displays the stabilities of CO_2 conversion with time on stream for inverse ZnO/Cu catalysts. For all the ZnO/Cu catalysts, no obvious decrease of conversion had been noticed for 50 h, suggesting no deactivation had taken place on them. CO and CH_3OH selectivity as well as CH_3OH yield are shown in Table 4. When the ZnO loading increased from 10 to 40%, CO_2 conversion and CH_3OH yield increased significantly. However, further increasing ZnO loading to 50%, CO_2 conversion and CH_3OH yield decreased to 8.9% and 2.4 mmol g^{-1} h^{-1}. Previously, Cu/ZnO had

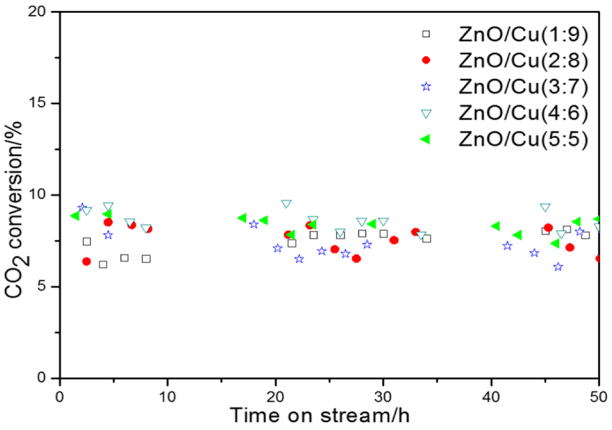

Fig. 7 Stabilities of CO_2 conversion with time on stream over the catalysts. Reaction conditions: 2.0 MPa, 250 °C, V_{H2}:V_{CO2} = 3:1, space velocity = 3.6 L·h^{-1}·g^{-1}

Table 4 Catalytic performance over ZnO/Cu catalysts at 2.0 MPa and 250 °C, V(H_2):V(CO_2) = 3:1, space velocity = 3.6 L h^{-1} g^{-1}

Sample	CO_2 conversion (%)	CO selectivity (mol%)	CH_3OH selectivity (mol%)	CH_3OH yield (mmol g^{-1} h^{-1})
ZnO/Cu(1:9)	7.5	72.1	27.9	0.8
ZnO/Cu(2:8)	8.0	65.7	34.3	1.1
ZnO/Cu(3:7)	8.3	58.3	41.7	1.3
ZnO/Cu(4:6)	8.9	40.8	59.2	2.1
ZnO/Cu(5:5)	8.4	59.9	40.1	1.4
Cu/ZnO (6:4)	13.5	65.7	34.3	1.8

been studied for methanol synthesis with different Cu/Zn ratios. Valant [29] reported that Cu/ZnO, with a Zn loading of 62%, exhibited the highest activity. The methanol formation rate was about 1.8 mmol g^{-1} h^{-1} at 3.0 MPa and 250 °C. Here, our results showed the best catalyst had a 2.8 mmol g^{-1} h^{-1} methanol yield, much higher than the reported one even at a lower reaction pressure. We also tested the Cu/ZnO catalyst with a Cu loading of 60%. CH_3OH yield was 1.8 mmol g^{-1} h^{-1}, much lower than the inverse ZnO/Cu sample with the same composition.

Discussion

Although many researchers have focused on the catalytic CO_2 hydrogenation using Cu–ZnO based catalysts in recent years, no agreement regarding the active phase of catalysts has been made. Some researchers believed that there was a strong interaction between the activity and the CuZn alloy [39, 45]. Some argued that CO_2 conversion

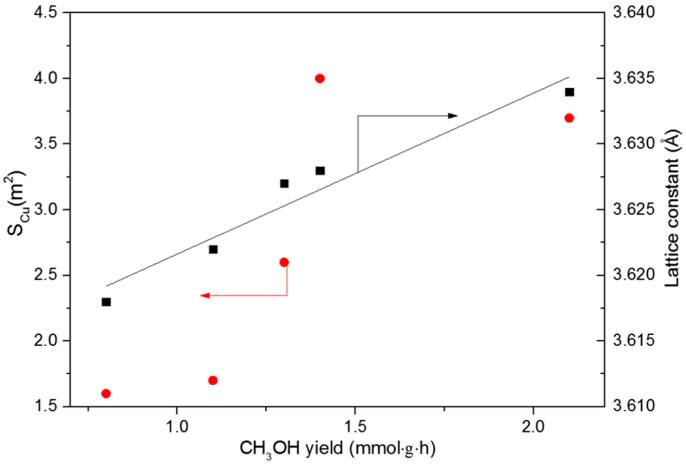

Fig. 8 The relationship between methanol yield and the exposed Cu surface area (obtained from the H_2-TPD results), Cu lattice constant (obtained from the XRD results) Reaction conditions: 2.0 MPa, 250 °C, V_{H2}:V_{CO2} = 3:1, space velocity = 3.6 L h^{-1} g^{-1}

was related to the Cu surface area [40, 46]. Still, others held the opinion that ZnO-Cu interfacial sites facilitated the methanol synthesis reaction [13, 47].

As shown in Fig. 8, methanol yield did not follow the trend of Cu surface area. This is also supported by the observation that Cu on its own is a poor catalyst for methanol synthesis from CO_2/H_2 [48]. Therefore, the surface area of Cu is not the factor for the methanol synthesis activity. Fig. 8 also shows the relationship between the Cu lattice constant and the yield of methanol. Clearly, a linear relationship can be detected. According to the Vegard's law [49], a linear relation exists between the crystal lattice constant of an alloy and the concentrations of the constituent elements. Therefore, it is reasonable to deduce that there is a linear relationship between the methanol yield and the CuZn alloy content.

Furthermore, the unique inverse structure inhabited the formation of highly dispersed Cu, of which the amount was much less than that of the conventional Cu/ZnO samples [50]. According to previous reports on the mechanism of CO_2 hydrogenation, H/D exchange experiments showed that the main side reaction (reverse water gas shift side reaction, $CO_2 + H_2 \rightarrow CO + H_2O$) proceeded on clean Cu surface sites [2, 51]. On Ce_xCu_yO [25], Cu/ZrO_2 and $Ga_2O_3/Cu/ZrO_2$ [52] catalysts, highly dispersed Cu sites were also considered the main active phases for reverse water gas shift reaction. Because of the lower amount of highly dispersed Cu sites on the surface, ZnO/Cu(4:6) sample had a lower CO selectivity and thus a higher methanol selectivity than Cu/ZnO (6:4).

Conclusions

Inverse ZnO/Cu catalysts were prepared with different Zn/Cu molar ratios and tested for CO_2 hydrogenation to methanol. The inverse structure made the Cu/Zn molar ratios on the surface much lower than in the bulk phase. CuZn alloy was formed in the samples and there is a linear relationship between the methanol yield and the CuZn alloy content. Highly dispersed CuO accounted for only a small amount on the surface, while large amount CuO was in the bulk form. ZnO/Cu(4:6) sample had the smallest Cu particle size and lowest CuO reduction peaks, indicating the strongest interaction between ZnO and CuO. In addition, the unique inverse structure inhabited the formation of highly dispersed Cu sites, which is helpful for the production of CO. As a result, ZnO/Cu(4:6) exhibited the highest CH_3OH yield (2.8 mmol g^{-1} h^{-1}) at 2.0 MPa and 250 °C. From the results, we reckoned that the inverse structure and the tuning of CuZn alloy content would be an important topic to guide the preparation of ZnO/Cu catalysts.

Acknowledgements We greatly acknowledge the National Natural Science Foundation of China (Grant 21303272) for the financial support. The Special Fund for Basic Scientific Research of Central Colleges, South-Central University for Nationalities (CZY19007) is also gratefully acknowledged.

References

1. Kirchner J, Zambrzycki C, Baysal Z, Güttel R, Kureti S (2020) Fe based core–shell model catalysts for the reaction of CO_2 with H_2. React Kinet Mech Cat 131(1):119–128. https://doi.org/10.1007/s11144-020-01859-9
2. Kunkes EL, Studt F, Abild-Pedersen F, Schlögl R, Behrens M (2015) Hydrogenation of CO_2 to methanol and CO on Cu/ZnO/Al_2O_3: Is there a common intermediate or not? J Catal 328:43–48. https://doi.org/10.1016/j.jcat.2014.12.016
3. Prašnikar A, Pavlišič A, Ruiz-Zepeda F, Kovač J, Likozar B (2019) Mechanisms of copper-based catalyst deactivation during CO_2 reduction to methanol. Ind Eng Chem Res 58(29):13021–13029. https://doi.org/10.1021/acs.iecr.9b01898
4. Kattel S, Yan B, Yang Y, Chen JG, Liu P (2016) Optimizing binding energies of key intermediates for CO_2 hydrogenation to methanol over oxide-supported copper. J Am Chem Soc 138(38):12440–12450. https://doi.org/10.1021/jacs.6b05791
5. Zhang X, Liu J-X, Zijlstra B, Filot IAW, Zhou Z, Sun S, Hensen EJM (2018) Optimum Cu nanoparticle catalysts for CO_2 hydrogenation towards methanol. Nano Energy 43:200–209. https://doi.org/10.1016/j.nanoen.2017.11.021
6. Karelovic A, Ruiz P (2015) The role of copper particle size in low pressure methanol synthesis via CO_2 hydrogenation over Cu/ZnO catalysts. Catal Sci Technol 5(2):869–881. https://doi.org/10.1039/c4cy00848k
7. da Silva RJ, Pimentel AF, Monteiro RS, Mota CJA (2016) Synthesis of methanol and dimethyl ether from the CO_2 hydrogenation over Cu·ZnO supported on Al_2O_3 and Nb_2O_5. J CO2 Util 15:83–88. https://doi.org/10.1016/j.jcou.2016.01.006
8. Kandemir T, Girgsdies F, Hansen TC, Liss KD, Kasatkin I, Kunkes EL, Wowsnick G, Jacobsen N, Schlogl R, Behrens M (2013) In situ study of catalytic processes: neutron diffraction of a methanol synthesis catalyst at industrially relevant pressure. Angew Chem Int Ed 52(19):5166–5170. https://doi.org/10.1002/anie.201209539
9. Fang X, Men Y, Wu F, Zhao Q, Singh R, Xiao P, Du T, Webley PA (2019) Promoting CO_2 hydrogenation to methanol by incorporating adsorbents into catalysts: effects of hydrotalcite. Chem Eng J 378:122052. https://doi.org/10.1016/j.cej.2019.122052

10. Li MM-J, Zeng Z, Liao F, Hong X, Tsang SCE (2016) Enhanced CO_2 hydrogenation to methanol over CuZn nanoalloy in Ga modified Cu/ZnO catalysts. J Catal 343:157–167. https://doi.org/10.1016/j.jcat.2016.03.020
11. Wang G, Mao D, Guo X, Yu J (2019) Methanol synthesis from CO_2 hydrogenation over CuO-ZnO-ZrO_2-M_xO_y catalysts (M=Cr, Mo and W). Int J Hydrogen Energy 44(8):4197–4207. https://doi.org/10.1016/j.ijhydene.2018.12.131
12. Lunkenbein T, Schumann J, Behrens M, Schlogl R, Willinger MG (2015) Formation of a ZnO overlayer in industrial Cu/ZnO/Al_2O_3 catalysts induced by strong metal-support interactions. Angew Chem Int Ed Engl 54(15):4544–4548. https://doi.org/10.1002/anie.201411581
13. Kattel S, Ramirez PJ, Chen JG, Rodriguez JA, Liu P (2017) Active sites for CO_2 hydrogenation to methanol on Cu/ZnO catalysts. Science 355(6331):1296–1299. https://doi.org/10.1126/science.aal3573
14. Rodriguez JA, Graciani J, Evans J, Park JB, Yang F, Stacchiola D, Senanayake SD, Ma S, Perez M, Liu P, Fdez Sanz J, Hrbek J (2009) Water-gas shift reaction on a highly active inverse CeO_x/Cu(111) catalyst: unique role of ceria nanoparticles. Angew Chem Int Ed 48(43):8047–8050. https://doi.org/10.1002/anie.200903918
15. Yang F, Js G, Evans J, Liu P, Hrbek J, Sanz JF, Rodriguez JA (2011) CO oxidation on inverse CeOx/Cu(111) catalysts: high catalytic activity and ceria-promoted dissociation of O_2. J Am Chem Soc 133(10):3444–3451. https://doi.org/10.1021/ja1087979
16. Ostroverkh A, Johánek V, Kúš P, Šedivá R, Matolín V (2016) Efficient ceria–platinum inverse catalyst for partial oxidation of methanol. Langmuir 32(25):6297–6309. https://doi.org/10.1021/acs.langmuir.6b01316
17. Palomino RM, Ramirez PJ, Liu Z, Hamlyn R, Waluyo I, Mahapatra M, Orozco I, Hunt A, Simonovis JP, Senanayake SD, Rodriguez JA (2018) Hydrogenation of CO_2 on ZnO/Cu(100) and ZnO/Cu(111) catalysts: role of copper structure and metal-oxide interface in methanol synthesis. J Phys Chem B 122(2):794–800. https://doi.org/10.1021/acs.jpcb.7b06901
18. Li CS, Melaet G, Ralston WT, An K, Brooks C, Ye Y, Liu YS, Zhu J, Guo J, Alayoglu S, Somorjai GA (2015) High-performance hybrid oxide catalyst of manganese and cobalt for low-pressure methanol synthesis. Nat Commun 6:6538. https://doi.org/10.1038/ncomms7538
19. Hinrichsen O, Genger T, Muhler M (2000) Chemisorption of N_2O and H_2 for the surface determination of copper catalysts. Chem Eng Technol 23:956–959
20. Fichtl MB, Schumann J, Kasatkin I, Jacobsen N, Behrens M, Schlogl R, Muhler M, Hinrichsen O (2014) Counting of oxygen defects versus metal surface sites in methanol synthesis catalysts by different probe molecules. Angew Chem Int Ed 53(27):7043–7047. https://doi.org/10.1002/anie.201400575
21. Van Der Grift CJG, AFHW, B. P. J. Joghi, J. Van Beijnum, M. De Boer, M. Versluijs-Helder, J. W. Geus, (1991) Effect of the reduction treatment on the structure and reactivity of silica-supported copper particles. J Catal 131:178–189
22. Zhao F, Gong M, Cao K, Zhang Y, Li J, Chen R (2017) Atomic layer deposition of Ni on Cu nanoparticles for methanol synthesis from CO_2 hydrogenation. ChemCatChem 9(19):3772–3778. https://doi.org/10.1002/cctc.201700622
23. Liao F, Huang Y, Ge J, Zheng W, Tedsree K, Collier P, Hong X, Tsang SC (2011) Morphology-dependent interactions of ZnO with Cu nanoparticles at the materials' interface in selective hydrogenation of CO_2 to CH_3OH. Angew Chem Int Ed 50(9):2162–2165. https://doi.org/10.1002/anie.201007108
24. Fujita S-i, Moribe S, Kanamori Y, Kakudate M, Takezawa N (2001) Preparation of a coprecipitated Cu-ZnO catalyst for the methanol synthesis from CO_2-effects of the calcination and reduction conditions on the catalytic performance. Appl Catal A 207:121–128
25. Zhou G, Dai B, Xie H, Zhang G, Xiong K, Zheng X (2017) CeCu composite catalyst for CO synthesis by reverse water–gas shift reaction: effect of Ce/Cu mole ratio. J CO2 Util 21:292–301. https://doi.org/10.1016/j.jcou.2017.07.004
26. Durupthy O, Bill J, Aldinger F (2007) Bioinspired synthesis of crystalline TiO_2 effect of amino acids on nanoparticles structure and shape. Cryst Growth Des 7(12):2696–2704. https://doi.org/10.1021/cg060405g
27. Álvarez Galván C, Schumann J, Behrens M, Fierro JLG, Schlögl R, Frei E (2016) Reverse water-gas shift reaction at the Cu/ZnO interface: influence of the Cu/Zn ratio on structure-activity correlations. Appl Catal B 195:104–111. https://doi.org/10.1016/j.apcatb.2016.05.007

28. Zhao F, Liu Z, Xu W, Yao S, Kubacka A, Johnston-Peck AC, Senanayake SD, Zhang A-Q, Stach EA, Fernández-García M, Rodriguez JA (2014) Water-gas shift reaction on Ni–W–Ce catalysts: catalytic activity and structural characterization. J Phys Chem C 118(5):2528–2538. https://doi.org/10.1021/jp410790z
29. Le Valant A, Comminges C, Tisseraud C, Canaff C, Pinard L, Pouilloux Y (2015) The Cu–ZnO synergy in methanol synthesis from CO_2, Part 1: Origin of active site explained by experimental studies and a sphere contact quantification model on Cu+ZnO mechanical mixtures. J Catal 324:41–49. https://doi.org/10.1016/j.jcat.2015.01.021
30. Nakamuraa J, Choia Y, Fujitanib T (2003) On the issue of the active site and the role of ZnO in Cu-ZnO methanol synthesis catalysts. Top Catal 22(3–4):277–285
31. Wang F, Liu Y, Gan Y, Ding W, Fang W, Yang Y (2013) Study on the modification of Cu-based catalysts with cupric silicate for methanol synthesis from synthesis gas. Fuel Process Technol 110:190–196. https://doi.org/10.1016/j.fuproc.2012.12.012
32. Zhao F, Liu Z, Xu W, Yao S, Si R, Johnston-Peck AC, Martínez-Arias A, Hanson JC, Senanayake SD, Rodriguez JA (2015) Pulse studies to decipher the role of surface morphology in CuO/CeO_2 nanocatalysts for the water gas shift reaction. Catal Lett 145(3):808–815. https://doi.org/10.1007/s10562-015-1482-y
33. Chu Z, Chen H, Yu Y, Wang Q, Fang D (2013) Surfactant-assisted preparation of $Cu/ZnO/Al_2O_3$ catalyst for methanol synthesis from syngas. J Mol Catal A 366:48–53. https://doi.org/10.1016/j.molcata.2012.09.007
34. Zhang Y, Zhong L, Wang H, Gao P, Li X, Xiao S, Ding G, Wei W, Sun Y (2016) Catalytic performance of spray-dried $Cu/ZnO/Al_2O_3/ZrO_2$ catalysts for slurry methanol synthesis from CO_2 hydrogenation. J CO_2 Util 15:72–82. https://doi.org/10.1016/j.jcou.2016.01.005
35. Din IU, Shaharun MS, Naeem A, Tasleem S, Rafie Johan M (2018) Carbon nanofibers based copper/zirconia catalysts for carbon dioxide hydrogenation to methanol: effect of copper concentration. Chem Eng J 334:619–629. https://doi.org/10.1016/j.cej.2017.10.087
36. Yang X, Chen H, Meng Q, Zheng H, Zhu Y, Li YW (2017) Insights into influence of nanoparticle size and metal-support interactions of Cu/ZnO catalysts on activity for furfural hydrogenation. Catal Sci Technol 7(23):5625–5634. https://doi.org/10.1039/c7cy01284e
37. Kuld S, Conradsen C, Moses PG, Chorkendorff I, Sehested J (2014) Quantification of zinc atoms in a surface alloy on copper in an industrial-type methanol synthesis catalyst. Angew Chem Int Ed Engl 53(23):5941–5945. https://doi.org/10.1002/anie.201311073
38. van den Berg R, Prieto G, Korpershoek G, van der Wal LI, van Bunningen AJ, Laegsgaard-Jorgensen S, de Jongh PE, de Jong KP (2016) Structure sensitivity of Cu and CuZn catalysts relevant to industrial methanol synthesis. Nat Commun 7:13057. https://doi.org/10.1038/ncomms13057
39. Kuld S, Thorhauge M, Falsig H, Elkjaer CF, Helveg S, Chorkendorff I, Sehested J (2016) Quantifying the promotion of Cu catalysts by ZnO for methanol synthesis. Science 352(6288):969–974. https://doi.org/10.1126/science.aaf0718
40. Gao P, Xie R, Wang H, Zhong L, Xia L, Zhang Z, Wei W, Sun Y (2015) Cu/Zn/Al/Zr catalysts via phase-pure hydrotalcite-like compounds for methanol synthesis from carbon dioxide. J CO_2 Util 11:41–48. https://doi.org/10.1016/j.jcou.2014.12.008
41. Waugh K (2004) The absorption and locking-in of hydrogen in copper. Solid State Ionics 168(3–4):327–342. https://doi.org/10.1016/j.ssi.2003.05.001
42. Millar GJ, Rochester CH, Bailey S, Waugh KC (1993) Combined temperature-programmed desorption and fourier-transform infrared spectroscopy study of CO, CO and H_2 interactions with model ZnO/SiO, Cu/SiO, and $Cu/ZnO/SiO_2$ methanol synthesis catalysts. J Chem Soc Faraday Trans 89(7):1109–1115
43. Ren H, Xu C-H, Zhao H-Y, Wang Y-X, Liu J, Liu J-Y (2015) Methanol synthesis from CO_2 hydrogenation over $Cu/\gamma\text{-}Al_2O_3$ catalysts modified by ZnO, ZrO_2 and MgO. J Ind Eng Chem 28:261–267. https://doi.org/10.1016/j.jiec.2015.03.001
44. Behrens M, Studt F, Kasatkin I, Kuhl S, Havecker M, Abild-Pedersen F, Zander S, Girgsdies F, Kurr P, Kniep BL, Tovar M, Fischer RW, Norskov JK, Schlogl R (2012) The active site of methanol synthesis over $Cu/ZnO/Al_2O_3$ industrial catalysts. Science 336(6083):893–897. https://doi.org/10.1126/science.1219831
45. Guo X, Mao D, Lu G, Wang S, Wu G (2011) The influence of La doping on the catalytic behavior of Cu/ZrO_2 for methanol synthesis from CO_2 hydrogenation. J Mol Catal A 345(1–2):60–68. https://doi.org/10.1016/j.molcata.2011.05.019

46. Lunkenbein T, Girgsdies F, Kandemir T, Thomas N, Behrens M, Schlögl R, Frei E (2016) Bridging the time gap: a copper/zinc oxide/aluminum oxide catalyst for methanol synthesis studied under industrially relevant conditions and time scales. Angew Chem Int Ed 55(41):12708–12712. https://doi.org/10.1002/anie.201603368
47. Senanayake SD, Ramírez PJ, Waluyo I, Kundu S, Mudiyanselage K, Liu Z, Liu Z, Axnanda S, Stacchiola DJ, Evans J, Rodriguez JA (2016) Hydrogenation of CO_2 to methanol on CeOx/Cu(111) and ZnO/Cu(111) catalysts: role of the metal–oxide interface and importance of Ce^{3+} sites. J Phys Chem C 120(3):1778–1784. https://doi.org/10.1021/acs.jpcc.5b12012
48. Denton AR, Ashcroft NW (1991) Vegard's law. Phys Rev A 43(6):3161–3164. https://doi.org/10.1103/PhysRevA.43.3161
49. Lei H, Hou Z, Xie J (2016) Hydrogenation of CO_2 to CH_3OH over $CuO/ZnO/Al_2O_3$ catalysts prepared via a solvent-free routine. Fuel 164:191–198. https://doi.org/10.1016/j.fuel.2015.09.082
50. Kattel S, Liu P, Chen JG (2017) Tuning selectivity of CO_2 hydrogenation reactions at the metal/oxide interface. J Am Chem Soc 139(29):9739–9754. https://doi.org/10.1021/jacs.7b05362
51. Fornero EL, Chiavassa DL, Bonivardi AL, Baltanás MA (2017) Transient analysis of the reverse water gas shift reaction on Cu/ZrO_2 and Ga_2O_3 /Cu/ZrO_2 catalysts. J CO_2 Util 22:289–298. https://doi.org/10.1016/j.jcou.2017.06.002